Roles of K149, G352, and H401 in the Channel Functions of ClC-0: Testing the Predictions from Theoretical Calculations

Xiao-Dong Zhang, Yong Li, Wei-Ping Yu, and Tsung-Yu Chen

Center for Neuroscience and Department of Neurology, University of California, Davis, CA 95616

The ClC family of Cl^- channels and transporters comprises membrane proteins ubiquitously present in species ranging from prokaryotes to mammals. The recently solved structures of the bacterial ClC proteins have provided a good model to guide the functional experiments for the eukaryotic Cl^- channels. Theoretical calculations based on the bacterial ClC structures have identified several residues critical for the Cl^- binding energy in the Cl^- transport pathway. It was speculated that the corresponding residues in eukaryotic Cl^- channels might play similar roles for the channel functions. In this study, we made a series of mutations in three such residues in eukaryotic ClC Cl^- channels (K149, G352, and H401 in ClC-0) and studied the functional consequences on the channel properties. A cysteine modification approach was also employed to evaluate the electrostatic effects of the charge placed at these three positions. The experimental results revealed that among the three residues tested, K149 plays the most important role in controlling both the gating and the permeation functions of ClC-0. On the other hand, mutations of H401 alter the channel conductance but not the gating properties, while mutations of G352 result in very little functional consequence. The mutation of K149 into a neutral residue leucine (K149L) shifts the activation curve and leads to flickery channel openings. The anion permeability ratios derived from bi-ionic experiments are also significantly altered in that the selectivity of Cl^- over other anions is decreased. Furthermore, removing the positive charge at this position reduces and increases, respectively, the accessibility of the negatively and positively charged methane thiosulfonate reagents to the pore. The control of the accessibility to charged MTS reagents and the regulation of the anion permeation support the idea that K149 exerts an electrostatic effect on the channel function, confirming the prediction from computational studies.

The Journal of General Physiology

INTRODUCTION

ClC chloride (Cl^-) channels and transporters play important roles in transporting Cl^- and protons (H^+) across the lipid membrane. This protein family includes Cl^- channels, such as ClC-0, ClC-1, and ClC-2 in the vertebrate species, as well as transporters such as *Escherichia coli* ClC-ec1 and some mammalian ClCs such as ClC-4 and ClC-5 (Maduke et al., 2000; Chen, 2005; Jentsch et al., 2005; Pusch and Jentsch, 2005). It has been recently shown that these transporters are Cl^- and H^+ antiporters; they shuffle Cl^- in exchange with H^+ across the lipid membrane (Accardi and Miller, 2004; Picollo and Pusch, 2005; Scheel et al., 2005). Although conventional views on ion channels and transporters are very different, the crystal structure of ClC-ec1 appears to serve as an excellent structural framework for interpreting the functional data obtained from vertebrate ClC channels (Estevez et al., 2003; Lin and Chen, 2003; Engh and Maduke, 2005). For example, several charged and uncharged residues important for the ClC-0 pore functions have their corresponding ClC-ec1 residues lining the Cl^- transport pathway (Ludewig et al., 1996; Middleton et al., 1996; Lin and Chen, 2000; Chen and Chen, 2003; Dutzler et al., 2003).

Theoretical studies based on the bacterial ClC structure showed that the energy profile encountered by Cl^- in the ion transport pathway was significantly influenced by those conserved pore residues (Bostick and Berkowitz, 2004; Cohen and Schulten, 2004; Corry et al., 2004; Faraldo-Gomez and Roux, 2004; Miloshevsky and Jordan, 2004). Fig. 1 depicts several critical positions of ClC protein molecules. T452 and E111 of ClC-ec1 (corresponding to K519 and E127 of ClC-0) are at the intracellular side, while R147 (K165 of ClC-0) is located at the extracellular side. The functional roles of their corresponding residues in ClC-0 have been demonstrated experimentally (Middleton et al., 1996; Lin and Chen, 2000; Chen and Chen, 2003). The negatively charged side chain of residue E148 (E166 of ClC-0) obstructs the pathway of Cl^- as if this side chain is acting as a "gate" to control the Cl^- transport process (Dutzler et al., 2002; Dutzler et al., 2003). In ClC-0, removing the negative charge of the corresponding glutamate residue greatly reduced the closing of the "fast gate" of the channel (Dutzler et al., 2003). In ClC-ec1, a mutation of E148 converted the Cl^--H^+ antiporter

Correspondence to Tsung-Yu Chen: tycchen@ucdavis.edu

Abbreviations used in this paper: HEK, human embryonic kidney; MTS, methane thiosulfonate; MTSEA, 2-aminoethyl MTS; MTSEH, 2-hydroxyethyl MTS; MTSES, 2-sulfonatoethyl MTS; WT, wild-type.

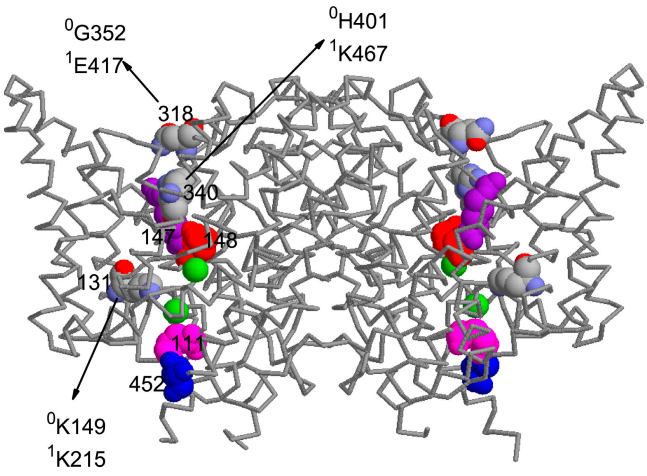

Figure 1. Amino acid residues that were experimentally or theoretically identified to be important for the functions of ClC proteins. Residues in red, purple, magenta, and blue have been experimentally shown to be critical for the pore function of ClC-0. Residues in CPK colors are those predicted to be important based on the ClC-ec1 structure. Their corresponding residues in ClC-0 and ClC-1 are shown as labeled by the numbers 0 and 1 at the left upper corner of the nomenclature.

behavior of the molecule into a uniporter, in which Cl^- flux is no longer coupled to the transport of H^+ (Accardi et al., 2004; Accardi and Miller, 2004).

In addition to these positions, several previously unexamined residues were identified by the theoretical studies based on bacterial ClC structures (Bostick and Berkowitz, 2004; Cohen and Schulten, 2004; Corry et al., 2004; Faraldo-Gomez and Roux, 2004; Miloshevsky and Jordan, 2004). These include N318 (corresponding to G352 and E417 of ClC-0 and ClC-1, respectively), R340 (corresponding to H401 and K467 of ClC-0 and ClC-1, respectively), and K131 (corresponding to K149 and K215 of ClC-0 and ClC-1, respectively; see Fig. 1 for their positions). Corry et al. (2004) suggested that the position of N318 might control the rate-limiting step of the Cl^- flux if the ion transport pathway of the bacterial ClC protein is opened to become an ion diffusion pore. Because the corresponding residues in ClC-0 and ClC-1 are glycine (a neutral amino acid) and glutamate (a negatively charged amino acid), respectively, the G to E change at this position may be responsible for the differences between ClC-0 and ClC-1 in the single-channel conductance and in the rectification properties of the open-channel I-V curve (Corry et al., 2004). Besides N318, the residues R340 and K131 were also proposed as contributors to the ion stabilization energy at the Cl^--binding sites based on theoretical calculations (Bostick and Berkowitz, 2004; Cohen and Schulten, 2004; Corry et al., 2004; Faraldo-Gomez and Roux, 2004; Miloshevsky and Jordan, 2004). A positive charge at these two positions was thought to stabilize the negatively charged permeant ion in the pore. The functional roles of the corresponding residues in vertebrate ClC channels, however, have not been examined.

To understand if the corresponding residues in vertebrate ClC channels also play critical roles, we mutated the residues corresponding to N318, R340, and K131 in vertebrate ClC channels. We examined the functional consequences of the channel properties upon mutations and also studied the influences of charge mutations on the modification rates of an introduced cysteine by methane thiosulfonate (MTS) reagents. The introduced cysteine to be modified was placed at position Y512 of ClC-0, which corresponds to Y445 of ClC-ec1, a residue that coordinates the bound Cl^- ion at the central Cl^--binding site (S_{cen}) (Dutzler et al., 2002, 2003). Because the electrostatic potential around a free thiol might affect the reactivity and accessibility of the thiol group to charged MTS reagents (Pascual and Karlin, 1998; Wilson et al., 2000; Lin and Chen, 2003), we used the MTS modification rate of Y512C to report the influence of these charge mutations on the electrostatic potential in the pore.

MATERIALS AND METHODS

Mutagenesis and Channel Expression

The functions of the ClC-0 Cl^- channel from the *Torpedo* electric organ are controlled by two gating mechanisms: the fast gating and the slow gating, which operate at the time scale of milliseconds and seconds, respectively (Maduke et al., 2000; Chen, 2005; Pusch and Jentsch, 2005). Only the fast-gating mechanism was involved in this study, so the slow gating of ClC-0 was suppressed by the point mutation C212S. This slow gating–suppressed mutant is identical to the wild-type (WT) channel for the other channel properties and is technically easier for data acquisition and interpretations (Lin et al., 1999). Therefore, all the mutations reported in this study were constructed in the background of C212S, which will be hereby referred to as the WT channel. The WT and mutant ClC-0 were constructed in pBluescript and pcDNA3. These two vectors were used for transient expressions of channels in *Xenopus* oocytes and human embryonic kidney (HEK) 293 cells, respectively. The WT human ClC-1, a gift from T. Jentsch (Hamburg University, Hamburg, Germany), was constructed in a vector pTLN. All mutations were made using PCR mutagenesis approaches, and the mutations were confirmed by commercially available DNA sequencing services. Synthesis of mRNA from the cDNA constructs and the injection of mRNA into *Xenopus* oocytes were performed according to previously described methods (Chen, 1998; Lin et al., 1999; Chen and Chen, 2001). Transfections of cDNA into HEK293 cells also followed a procedure described before (Lin and Chen, 2003). Normally, the channels were recorded 1–5 d after mRNA was injected to the oocytes or cDNA was transfected into the HEK 293 cells.

Electrophysiological Recordings

Two heterologous expression systems (*Xenopus* oocytes and HEK293 cells) were used in this study for different purposes. It is easier to control the channel density expressed on the oocyte membrane through injections of the adjusted concentrations of mRNAs. Therefore, single-channel recording experiments were performed using channels expressed in *Xenopus* oocytes. On the other hand, the current expression level in excised membrane patches appears to be larger in HEK 293 cells. Therefore, macroscopic current recordings from excised patches (such as in the

MTS modification experiments) were performed in HEK293 cells. Various electrophysiological recording methods used in this study have all been described previously (Chen, 1998; Lin et al., 1999; Lin and Chen, 2000; Chen and Chen, 2001, 2003). In brief, three different types of recordings were employed: two-electrode voltage clamp techniques for recording whole oocyte current, excised inside-out patch recordings of oocyte membranes for single-channel experiments, and macroscopic current recordings from the excised inside-out membrane patches of HEK 293 cells. For two-electrode voltage clamp recordings, the control of the membrane potential was achieved by a voltage clamp amplifier (725C, Warner Instruments/Harvard Apparatus). Data acquisition was performed by a Pentium PC computer equipped with a Digidata 1200 analogue interface, using pClamp6 software (Axon Instruments/Molecular Device). The electrodes were filled with 3 M KCl and had a resistance <1 MΩ. The standard recording (extracellular) solution was ND96 solution, containing (in mM) 96 NaCl, 2 KCl, 1 $MgCl_2$, 0.3 $CaCl_2$, 5 HEPES, pH 7.5. In Fig. 4, solutions of various Cl^- concentrations (100, 20, 4, and 1 mM) were used. These solutions contained (in mM) 100X NaGlu, X NaCl, 2 MgSO4, 5 HEPES, pH 7.5, where X represents the Cl^- concentration.

For recording single channels, the membrane voltage was controlled by the Axopatch 200B patch clamp amplifier (Axon Instruments/Molecular Device). The recorded traces were first filtered by a low-pass analogue filter (−3dB 200 Hz), and were digitized at 1 kHz by a digitizing board (DAP800, Microstar Inc.) controlled by a homemade acquisition program (Chen and Miller, 1996; Chen and Chen, 2003; Chen et al., 2003). The pipette (extracellular) solution contains (in mM) 140 NMG-Cl, 1 $CaCl_2$, 5 HEPES, pH 7.5. The bath (intracellular) solution contains (in mM) 140 NaCl, 1 EGTA, 5 HEPES, pH 7.5.

The macroscopic current recordings from excised inside-out patches of HEK293 cells were also conducted using the Axopatch 200B patch-clamp amplifier. The recording trace was digitally filtered at 1 kHz, and the signal was digitized at 2 kHz using Digidata 1320 digitizing board and pClamp8 software (Axon Instruments/Molecular Device). Both the pipette and the bath solutions contained (in mM) 130 NaCl, 5 $MgCl_2$, 5 HEPES, 1 EGTA, pH 7.4. The pipette resistance was ∼1–3 MΩ, and the series resistance was not corrected.

For macroscopic current recordings, a voltage protocol was used throughout the study to examine the fast-gate open probability (P_o) of the channel (Chen, 1998; Lin et al., 1999; Lin and Chen, 2000, 2003; Chen and Chen, 2001). Normally, this standard voltage protocol started with a positive prepulse (at +60 or +80 mV) voltage step followed by different test voltages from +60 or +80 mV to −160 mV in −20-mV steps. For K149 mutants, because the P_o-V curve was shifted >80 mV toward the depolarization direction, the test voltage started at +160 or +180 mV so that the true maximal P_o at such a potential was close to unity. Following the test voltage pulse, a −100-mV voltage step was applied to measure the tail current, and the relaxation process of the tail current was fitted to a single-exponential function. The instantaneous tail current was determined by extrapolating the tail current to the beginning of the tail pulse.

To examine the relative permeability ratios of various anions to Cl^-, the reversal potentials of the recorded currents from excised inside-out patches were measured under bi-ionic conditions. In this particular experiment the pipette (extracellular) solution contained (in mM) 140 NaCl, 5 HEPES, 1 EGTA, pH 7.4. The bath (intracellular) solution had the same content as the pipette solution, except that NaCl was replaced with the same concentration of NaX, where X represents the substituted anion.

MTS Modifications

All MTS modification experiments were conducted in excised inside-out patches from HEK293 cells. For controls, the three MTS reagents used in this study, 2-sulfonatoethyl MTS (MTSES), 2-hydroxyethyl MTS (MTSEH), and 2-aminoethyl MTS (MTSEA) had no effect on the WT ClC-0 channel (not depicted). These MTS reagents were purchased from Toronto Research Chemicals, Inc. Stock solutions of 0.3 M were first made and stored in a −80°C freezer. The working solutions containing the required MTS reagents were made from the stock solution immediately before use. The solution exchange was achieved using a fast solution exchanger (SF-77, Warner Instrument). The membrane potential of the patch was clamped at −40 mV when the patch was exposed to the MTS reagents (V_{MO} = −40 mV). The current of the patch was monitored at +80 mV (V_{MN} = +80 mV). Detailed procedures of the solution exchange and the experimental protocols were described previously (Lin and Chen, 2003).

Data Analysis

Although ClC-0 contains two identical pores, as suggested from the equally spaced three current levels in single-channel recording traces, the functions of the two fast gates of the channel are independent of each other (Miller, 1982; Hanke and Miller, 1983; Miller and White, 1984; Bauer et al., 1991; Chen and Miller, 1996; Ludewig et al., 1996; Middleton et al., 1996; Saviane et al., 1999; Lin and Chen, 2000; Chen and Chen, 2003). Therefore, the fast-gate P_o can be estimated from a single pore. At the macroscopic current level, the fast gating is represented by the current deactivation that results from a decrease of the fast-gate P_o upon membrane hyperpolarization. Using the standard voltage protocol described above, the fast-gate P_o can be estimated by normalizing the instantaneous tail current following various testing voltages to the maximal value obtained at the most depolarized test potential (+80 mV, or +180 mV in K149 mutants). The half-activating voltage was estimated by fitting the P_o-V curve to a Boltzmann equation. To estimate the opening and closing rates of the fast gate, the time constant (τ) of the current deactivation at different test voltages was also determined by fitting the current relaxation to a single-exponential function. The opening (α) and closing (β) rates are then calculated according to Eqs. 1a and 1b:

$$\alpha = P_o / \tau \tag{1a}$$

$$\beta = (1 - P_o) / \tau. \tag{1b}$$

The single-channel current amplitude was determined from the all-points amplitude histogram of the single-channel recording trace as shown in the previous work (Lin and Chen, 2000; Chen and Chen, 2001). The estimated single-channel current was plotted as a function of membrane voltages to construct the single-channel i-V plot. In Fig. 7 C, when estimating the gating kinetics from the WT single-channel recording traces, the trace was further digitally filtered at 200Hz, resulting in a final corner frequency of ∼140 Hz. For the single-channel trace of K149L, because of the flickery opening events, the burst and interburst durations (corresponding to the opening and closing events of the WT channel) were analyzed by digitally filtering the trace at 50 Hz (final corner frequency 40 Hz). As will be seen in the results, the calculated opening and closing rates of the mutant are still below this corner frequency.

Macroscopic I-V curves were used to compare the rectification properties of the WT and mutant channels. The open-channel current was determined from the instantaneous current at different voltages immediately following the prepulse at which the P_o of the fast gate was unity. The values at different voltages were normalized to the absolute current value obtained at −100 mV, and data from different cells or patches were then averaged. The rectification index was calculated by taking the ratio of the open-channel current at +80 mV versus the absolute value at −80 mV.

To calculate the permeability ratio (P_X/P_{Cl}, X represents an anion other than Cl^-) from the bi-ionic experiments, the reversal potential (E_{rev}) of the recorded current was determined by interpolating the zero-current potential in the I-V curve from the two voltages at which the current showed opposite signs. Junction potentials were <5 mV and were corrected. The permeability ratio was then determined according to Eq. 2:

$$P_X/P_{Cl} = \exp(E_{rev} \cdot F/RT), \quad (2)$$

where F, R, and T are Faraday constant, gas constant, and absolute temperature, respectively.

To estimate the MTS modification rate (k_{MTS}), the current measured at +80 mV at each voltage sweep was normalized to that measured right before the application of MTS reagents. The current decreasing process upon MTS modification was fitted to a single-exponential function. The time constant (τ_{mo}) and the concentration of MTS reagents ([MTS]) were used to calculate the modification rate constant according to Eq. 3:

$$k_{MTS} = 1/(\tau_{mo} \cdot [MTS]). \quad (3)$$

Statistics were conducted using Origin software (OriginLab, Co.). All results are presented as mean ± SEM.

RESULTS

Charge Mutations for G352 of ClC-0 (and E417 of ClC-1)

The amino acid that corresponds to N318 of ClC-ec1 is not conserved throughout the ClC family members. In ClC-0 and ClC-1, the corresponding residues are G352 and E417 respectively (Dutzler et al., 2002). By applying a harmonic force to expand the Cl^- transport pathway, Corry et al. (2004) converted the Cl^- transport pathway of ClC-ec1 into an ion diffusion pore. They suggested that the charge difference at this position could lead to the different ion permeation properties between ClC-0 and ClC-1. In particular, a negative charge at this position (glutamate) was thought to be responsible for the inwardly rectified I-V curve of ClC-1. To test this idea,

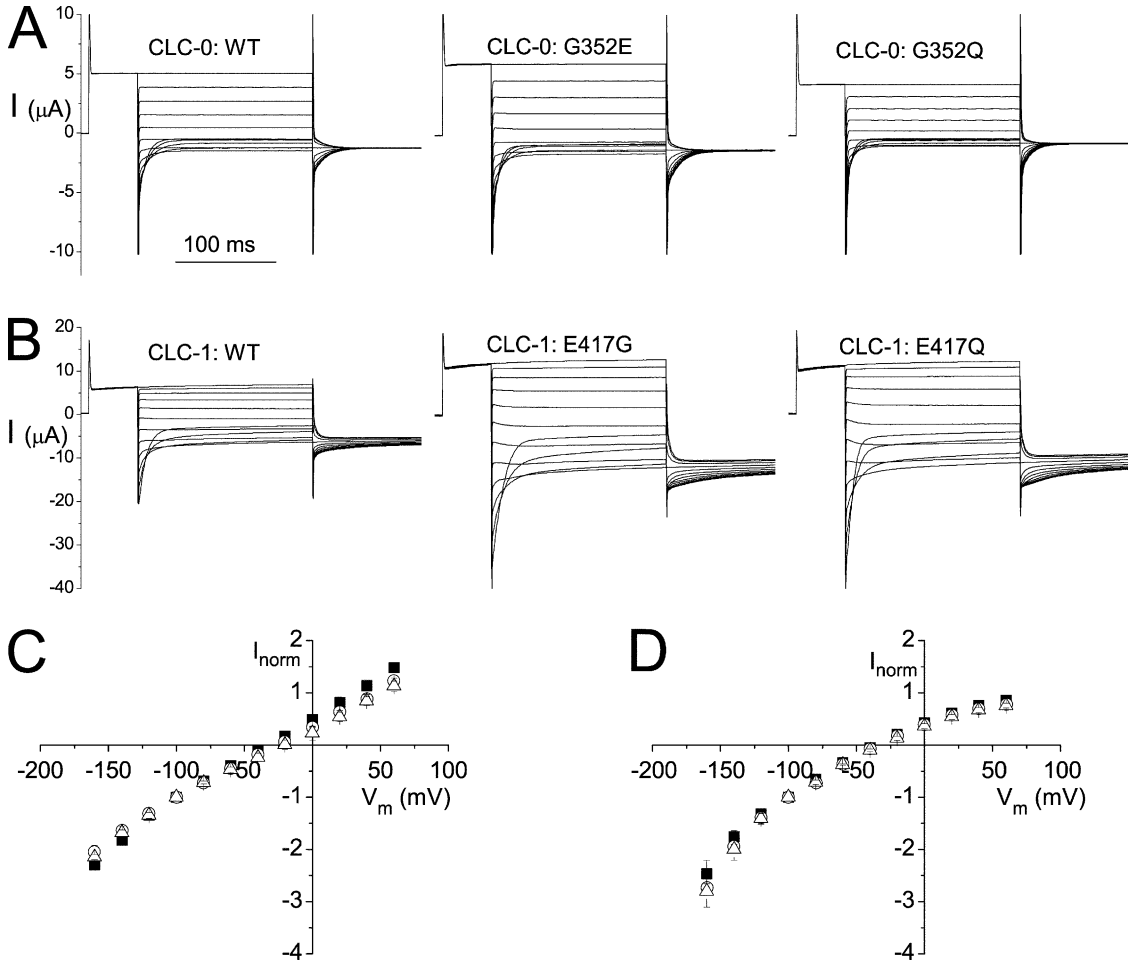

Figure 2. Functional roles of G352 of ClC-0 and E417 of ClC-1. (A) Whole oocyte current recordings for the WT ClC-0 and the G352E and G352Q mutants of ClC-0. Experiments were performed in the ND96 solution using the standard voltage protocol. (B) Whole oocyte recordings for the WT ClC-1 and the E417G and E417Q mutants of ClC-1. Same recording voltage protocols and solutions as those in A. (C) Instantaneous I-V relations for the three channels shown in A. Symbols are: filled squares, WT ClC-0; open circles, G352E; open triangles, G352Q. (D) Instantaneous I-V curve for the three channels shown in B. Symbols are: filled squares, WT ClC-1; open circles, E417G; open triangles, E417Q.

we swapped the two residues G and E between ClC-0 and ClC-1 and compared the pore properties between the WT and the mutant channels (Fig. 2). Fig. 2 (A and B) shows the recording traces of the WT channels and several mutants for ClC-0 and ClC-1, respectively. The comparisons of the instantaneous I-V curves between the mutant channels and the WT channels for ClC-0 and ClC-1 are shown in Fig. 2 (C and D). For ClC-1, removal of the negative charge at this position (either E to G or E to Q mutation) does not change the inward rectification of the I-V curve (Fig. 2 D). For ClC-0, although G352E mutation appears to slightly reduce the outward current, this phenomenon is also observed in G352Q mutant (Fig. 2 C), a mutation that does not change the charge of the side chain. We thus conclude that the charge difference at this position is not responsible for the difference in the open-channel current rectification between ClC-0 and ClC-1.

Another prediction of the G to E variation at this position between ClC-0 and ClC-1 is that the charge difference may result in the different single-channel conductance seen in ClC-0 and ClC-1; the single-channel conductance of ClC-0 and ClC-1 (~10 pS and 1.5 pS, respectively) differs by approximately sevenfold. Converting G352 of ClC-0 to a negatively charged residue, however, does not reduce the single-channel conductance of ClC-0 (Fig. 3, A and B). N318 of ClC-ec1 was also suggested to be important to stabilize Cl^- at a low-affinity Cl^--binding site at the very external end of the Cl^- transport pathway, called S^*_{ext} (Faraldo-Gomez and Roux, 2004). This Cl^--binding site was thought to correspond to the one responsible for the depolarization-activated channel opening in ClC-0, as hypothesized by Chen and Miller (1996). If the corresponding residue in ClC-0 is also critical in stabilizing the Cl^--binding to S^*_{ext}, a charge mutation at this position is expected to alter the external Cl^--dependent fast gating. Fig. 3 C shows that this appears not to be the case because WT ClC-0 and the G352E mutant show nearly identical fast-gating properties. Thus, the G352E mutation of ClC-0 generates minimal functional consequences in both the gating and permeation properties of the channel.

Functional Consequences of H401E Mutation in ClC-0

R340 of ClC-ec1 does not line the Cl^- transport pathway. However, like N318, it was suggested that a positive charge at this position could influence the stabilization of Cl^- binding at S^*_{ext} (Faraldo-Gomez and Roux, 2004).

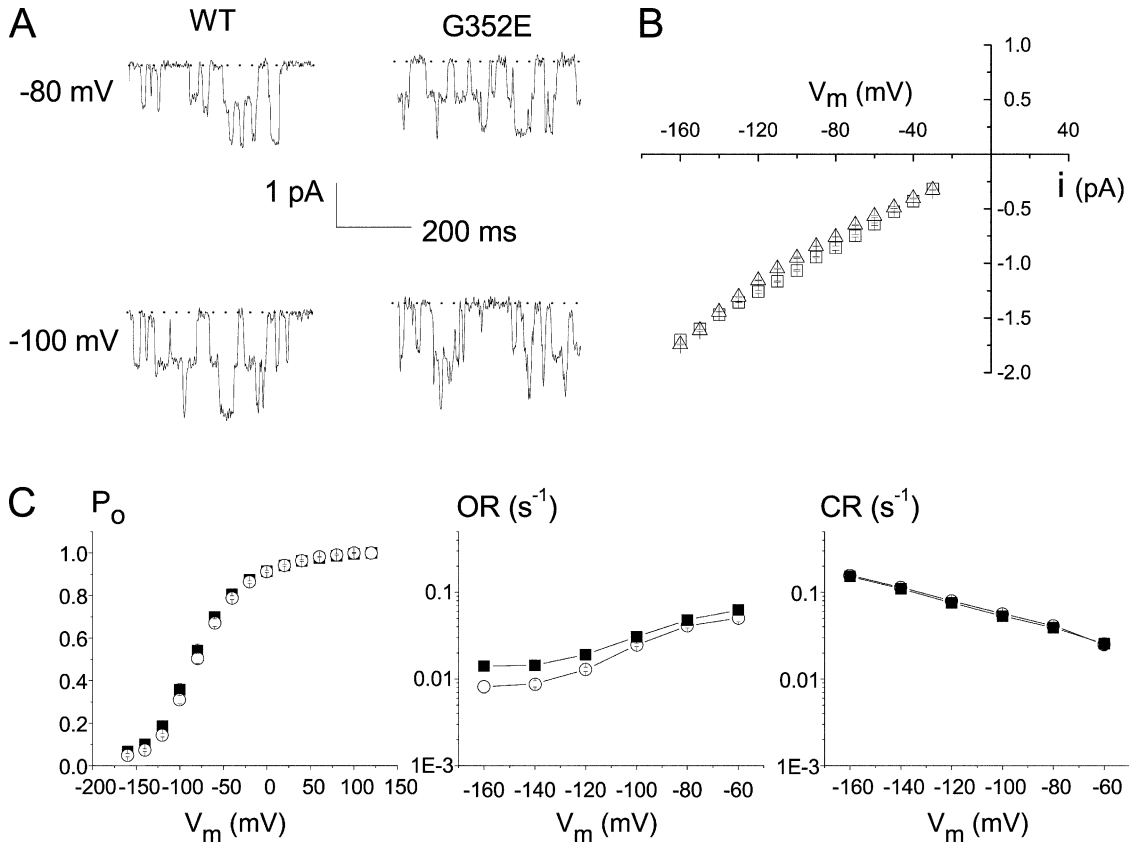

Figure 3. Permeation and gating properties of G352E of ClC-0. (A) Single channel recordings of the WT ClC-0 and the G352E mutant of ClC-0 at two voltages. (B) Single-channel i-V relationships for the WT ClC-0 (open squares) and the G352E mutant (open triangles). (C) Comparing gating parameters (P_o, open probability; OR, opening rate; CR, closing rate) of WT ClC-0 (filled squares) and the G352E mutant (open circles).

In ClC-0, the corresponding residue is histidine (H401). If this residue is critical to a Cl^--binding site responsible for the Cl^--dependent fast gating, a charge mutation at this position should affect the fast-gating mechanism of ClC-0. Fig. 4 (A and B) shows the macroscopic current recordings of WT ClC-0 and the H401E mutant, respectively, in the presence of 100 or 4 mM extracellular Cl^- concentration ($[Cl^-]_o$). The shifts of P_o-V curves in response to different $[Cl^-]_o$ are compared in Fig. 4 (C and D). It is clear that the fast-gate P_o-V curve of the H401E mutant at the physiological Cl^- concentration is almost identical to that of the WT channel. The right shifts of the P_o-V curves in the WT and mutant channels in response to the reduction of $[Cl^-]_o$ are also identical. Thus, the functional role of H401 in the $[Cl^-]_o$-dependent gating mechanism of ClC-0 cannot be confirmed.

Although the H401E mutation produces very little effect on the gating of ClC-0, this mutation significantly alters the ion permeation properties of the channel. Fig. 5 compares the single-channel recording traces of WT ClC-0 and the H401E mutant in the presence of 140 mM symmetrical Cl^- concentrations. The single-channel i-V plots for these two channels show that the conductance of H401E mutant is ~5 pS, while that of the WT ClC-0 is ~10 pS. Compared with the WT ClC-0, the H401E mutant also shows a slight inward rectification in the single-channel i-V curve (compare the single-channel current at −80 and −160 mV in the bottom panel of Fig. 5). This rectification property can be more clearly seen from a macroscopic I-V curve. Fig. 6 (A–C) shows the macroscopic current recordings of the WT channel as well as G352E and H401E mutants obtained from excised inside-out patches in the presence of symmetrical 140 mM Cl^-. In these experiments, the open-channel current was measured in a full range of membrane potential (from +80 to −160 mV). The macroscopic I-V curves for the instantaneous currents are also shown in each panel. The degree of rectification was quantified by calculating the ratio of the absolute current amplitude at +80 mV versus that at −80 mV, a property called rectification index. Fig. 6 D shows that the mutation of H401E yields a change of the rectification index from a value of ~0.8 in the WT channel to a value of ~0.5. These functional changes

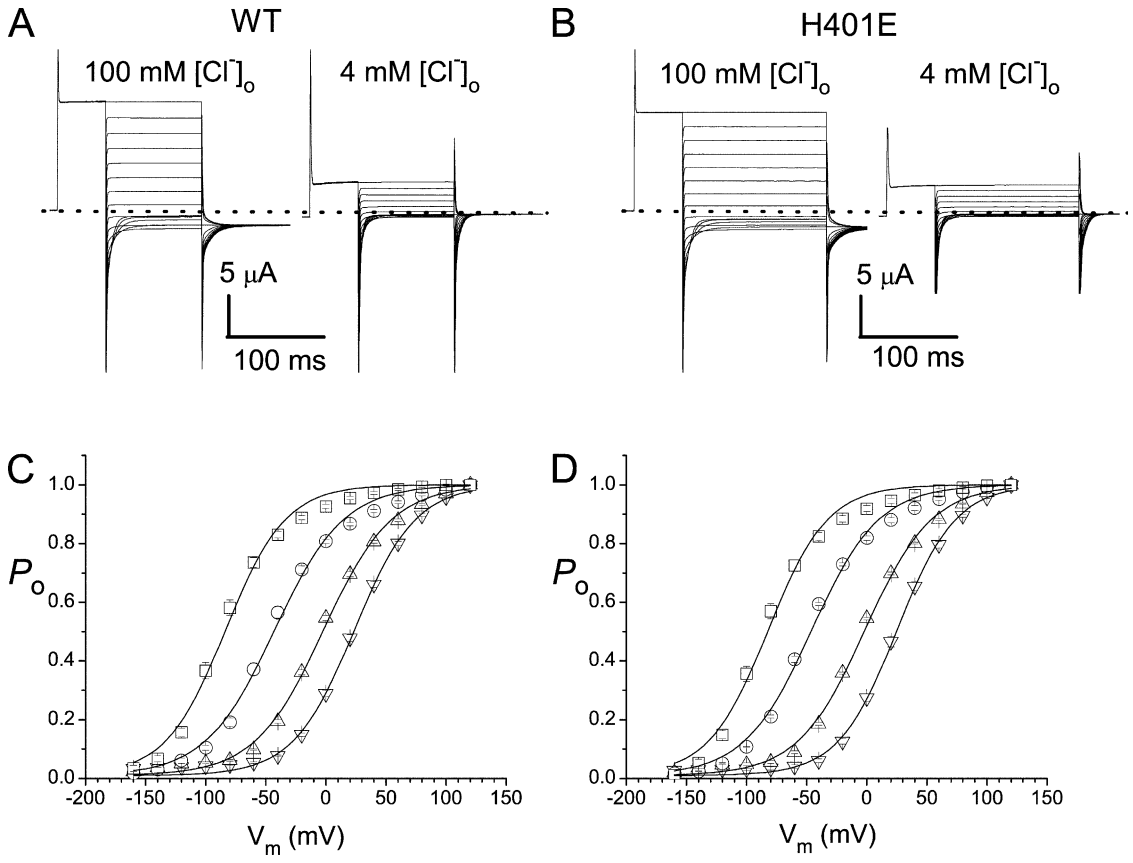

Figure 4. Gating effects of extracellular Cl^- between WT ClC-0 and the H401E mutant. (A) Macroscopic current recordings of WT ClC-0 in 100 and 4 mM $[Cl^-]_o$ solutions. Dotted line represents the zero-current level. (B) Macroscopic current recordings of H401E mutant of ClC-0 in 100 and 4 mM $[Cl^-]_o$ solution. (C) Steady-state P_o-V curves of WT ClC-0 in 100 (squares), 20 (circles), 4 (up triangles), and 1 mM (down triangles) $[Cl^-]_o$. (D) Steady-state P_o-V curves of H401E mutant. Experimental conditions and symbols are the same as those in C.

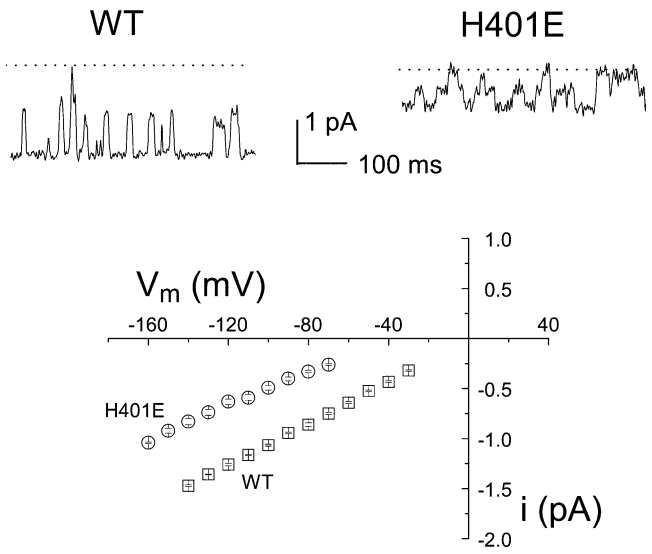

Figure 5. Single-channel i-V curves of the H401E mutant and the WT ClC-0. Real-time recording traces are compared in the top panel. The recordings were performed with nearly symmetrical Cl^- solutions on both sides of the membrane (142 vs. 140 mM Cl^- in the pipette and bath solutions, respectively). $V_m = -100$ mV. The comparison of single-channel i-V curves between WT ClC-0 and H401E mutant is shown in the bottom panel.

in ion permeation properties are consistent with the theoretical calculation in ClC-ec1, in which the charge at the R340 position may affect the stabilizing energy for Cl^- binding to the ion transport pathway (Faraldo-Gomez and Roux, 2004). On the other hand, a charge alteration at position N318 (G352 of ClC-0) appears to have little effect on the open-channel current rectification.

K149 Mutations Severely Alter the Gating and Permeation Functions of ClC-0

One intriguing finding from theoretical calculations was the electrostatic contribution of K131 in stabilizing the Cl^- binding to all three binding sites in ClC-ec1 (Faraldo-Gomez and Roux, 2004) despite the fact that the side chain of K131 does not directly line the ion transport pathway. Faraldo-Gomez and Roux's calculations pointed out that the single most important favorable ion–side chain electrostatic interaction in ClC-ec1 originates not from the ion-contacting residues such as S107 or Y445 but from K131 (Faraldo-Gomez and Roux, 2004). A lysine residue at this position is conserved from the bacterial to the mammalian ClC proteins. To examine the functional role of the corresponding lysine residue (K149) in ClC-0, we constructed several K149 mutants, including K149E, K149D, K149A, K149L, and K149R. We have so far been unable to functionally express K149E in *Xenopus* oocytes. Two runs of expression of K149E and K149D mutants in HEK293 cells did not result in functional current within 5 d of transfections using excised patch recording methods. On the other hand, the expression of K149L, K149R, and K149A mutants was robust. The recording traces of these three mutants expressed in *Xenopus* oocytes are shown in Fig. 7 A. The comparisons of the steady-state

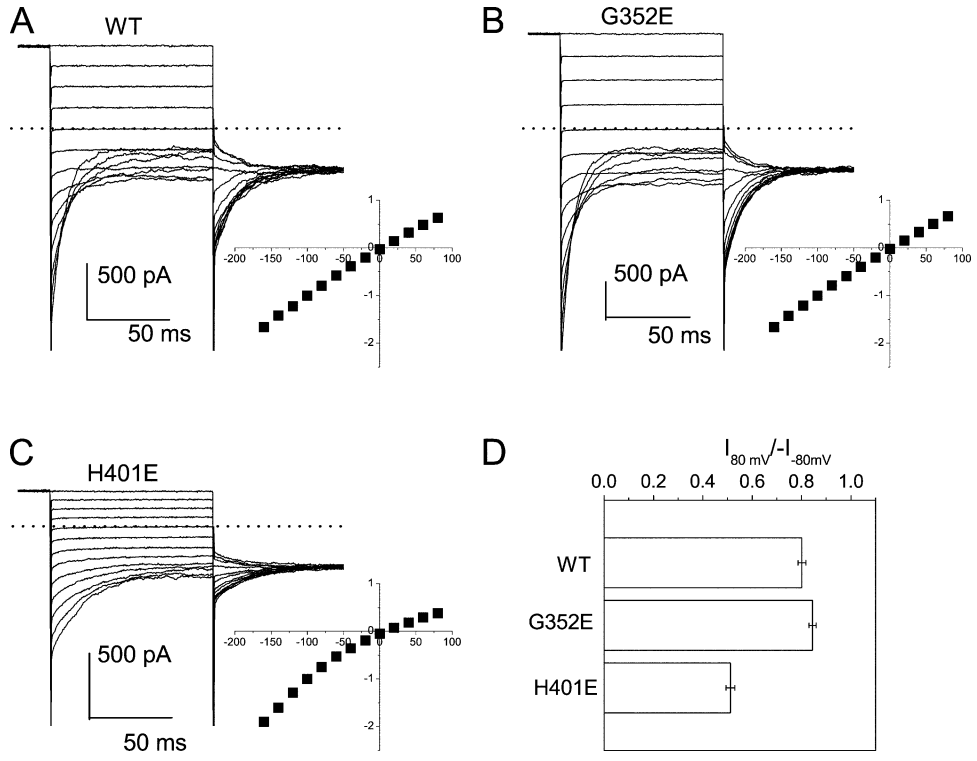

Figure 6. H401E, but not G352E mutant, shows inward current rectification when comparing with the WT ClC-0. (A) Macroscopic current recording of WT ClC-0 from an excised inside-out patch. Inset, instantaneous I-V curve of WT ClC-0 from the average of five patches. Symmetrical 140 mM Cl^- solutions on both sides of the membrane. (B) Macroscopic current recordings of G352E mutant in an excised inside-out patch. (C) Macroscopic current recordings of H401E mutant. Insets in B ($n = 8$) and C ($n = 10$) are the same as that in A. (D) Rectification indices of WT, G352E, and H401E mutants.

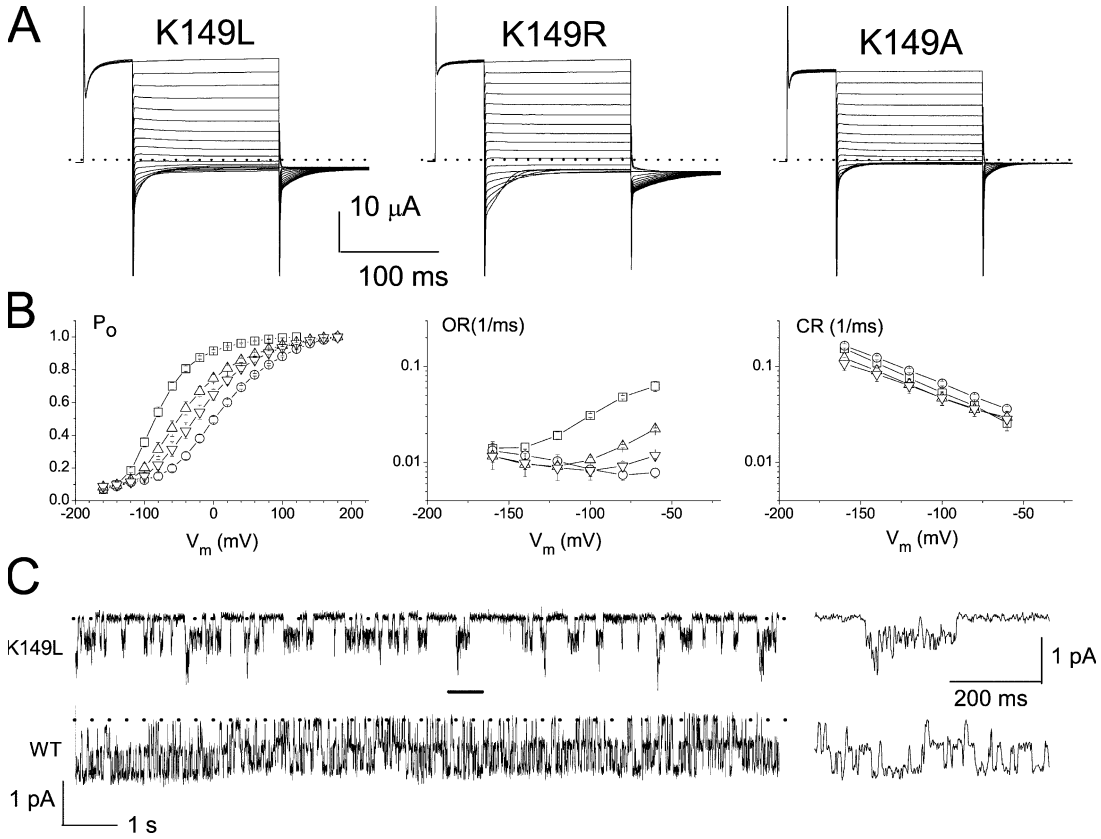

Figure 7. Effects of K149 mutations on the ClC-0 fast gating. (A) Whole oocyte recordings of K149L, K149R, and K149A mutants. Test voltages were from +180 to −160 mV. (B) Steady-state P_o-V curves (left), opening rate curves (middle), and closing rate curves (right) derived from experiments as shown in A. Symbols are: squares, WT ClC-0; up triangles, K149R; down triangles, K149A; circles, K149L. For opening and closing rate, data at voltages equal to or above −40 mV are not available because the time constant of the deactivation process cannot be reliably measured. (C) Single-channel recording traces of the K149L mutant and the WT channel at −50 mV. The 500-ms recording trace indicated by the horizontal bar is expanded to the right of each trace.

P_o-V curve, the opening-rate curve, and the closing-rate curve in standard ND96 solution of these three channels with those of the WT channel are shown in Fig. 7 B. It can be seen that the P_o-V curves of all three K149 mutants are significantly shifted to the more depolarized potential. The half-activation voltages for the WT channel, K149R, K149A, and K149L in regular ND96 solution are −78, −41, −20, and +8 mV, respectively (Fig. 7 B, left). This shift in P_o-V curve is mostly due to an effect on the opening rate of the fast gate (Fig. 7 B, middle and right). We have tried single-channel recordings for the K149L mutant, a challenging task due to the altered gating kinetics. Fig. 7 C shows a comparison of single-channel traces between K149L and the WT channel. An unexpected finding from the K149L mutant is that the channel opening events exhibit flickery behaviors, a phenomenon that, although beyond the scope of this study, deserves further investigations. At the same time, the mean current of each protopore is reduced to ∼80% of that of the WT channel (0.45 vs. 0.54 pA from the mutant and WT traces, respectively; amplitude histograms not shown). The small opening rate of this mutant can be directly seen from the long closed events (the interval between the bursts of channel activity) when compared with those in the WT recording trace (Fig. 7 C). Single-channel analyses show that the state probabilities of the three current levels of this mutant still follow a binomial distribution. The channel's P_o, opening rate, and closing rate (based on the burst and interburst durations, respectively) from this particular trace (a 46-s trace in total) are 0.14, 4.1 s^{-1}, and 24.6 s^{-1}, respectively. In comparison, the three parameters derived from the shown WT trace are 0.66, 60.4 s^{-1}, and 31.0 s^{-1}, respectively. Two other patches of the K149L mutant showed similar gating kinetics. These numbers are roughly consistent with those values projected from the macroscopic current recordings (Fig. 7 B).

To further understand the role of K149 in anion permeation, we examined the permeability ratios of various anions. Fig. 8 shows the recordings obtained in various bi-ionic conditions. The reversal potentials of these recordings and the derived relative permeability ratios were determined (Table I). It can be seen that the relative permeability ratios of different anions are all

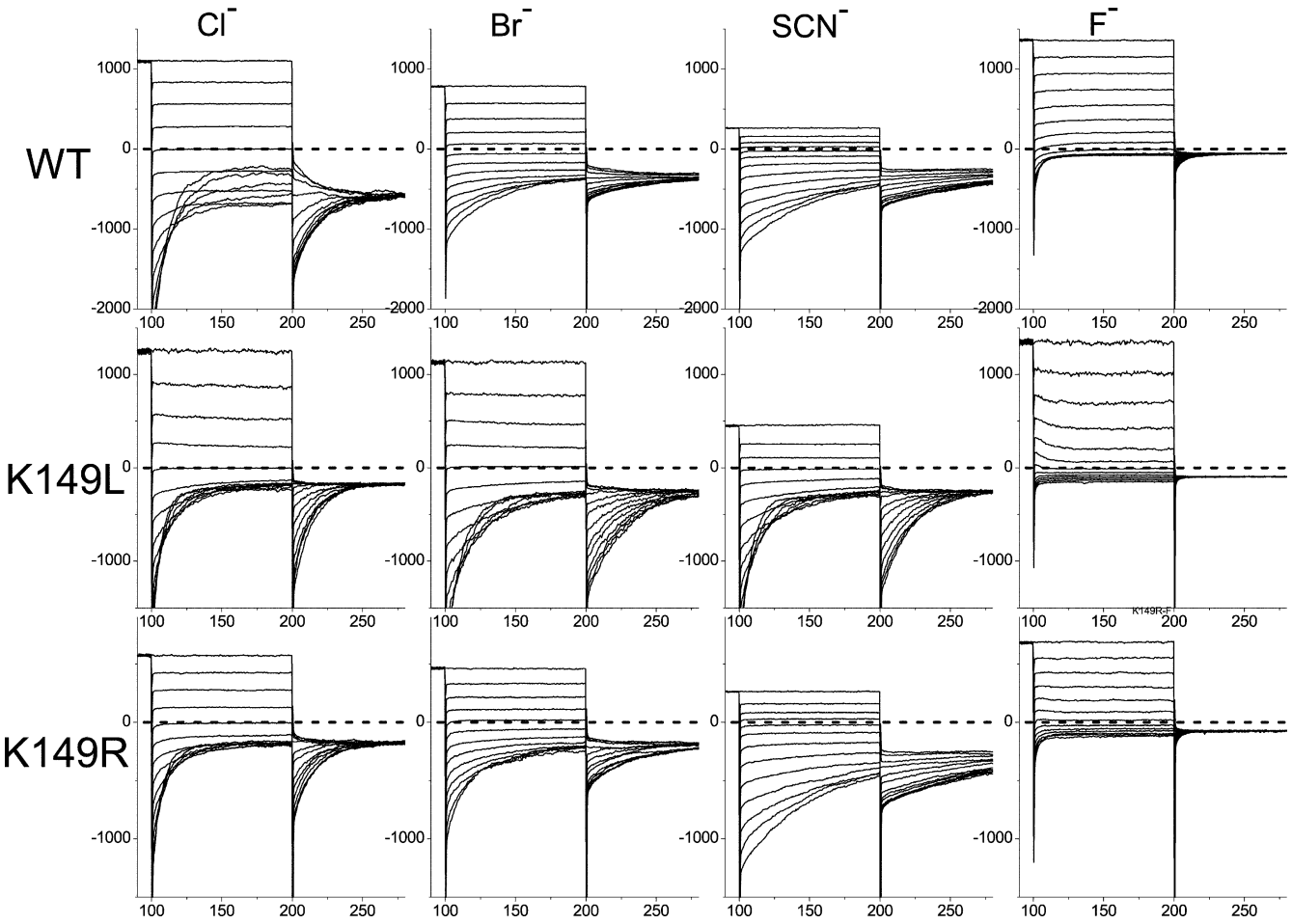

Figure 8. Macroscopic current recordings of WT CLC-0 and the K149L and K149R mutants in excised inside-out patches under bi-ionic conditions. The pipette solution contained 140 mM Cl^- while the bath solution contained the same concentration of the indicated ion. Voltages of the test pulse were from +80 mV to −160 mV in −20 mV steps, and the voltage of the tailed pulse was −100 mV. In each panel the vertical axis represents current in pA while the horizontal axis represents time in ms. The prepulse current is only shown for the final 10 ms. Dashed lines indicate the zero-current level.

significantly increased in the K149L mutant. For most of the anions, the permeability ratio in K149R is between those of the WT channel and the K149L mutant. These results are consistent with the mutational effects on the channel gating in which the P_o-V curve of K149R is right shifted to a degree less than that of the K149L mutation. The consistency in the degree of the gating versus the permeation effects resulted from the K149R and K149L mutations may reflect the intimate gating-permeation coupling of ClC-0.

Effects of Charge Mutations Reported by the MTS Modification of Y512C

Although the channel behaviors of mutants of K149 significantly deviate from those of the WT channel, interpreting the functional role of the mutated residue is still limited because the mutational consequence could result from either a structural or an electrostatic perturbation. To evaluate the electrostatic effects of mutations, we employed the MTS modification experiments. Previous work has shown that Y512C of ClC-0 can be reached by MTS reagents applied from the intracellular side (Lin and Chen, 2003; Engh and Maduke, 2005). The modification rate of an introduced cysteine depends on two general variables, the accessibility and the reactivity of the free thiol group (Pascual and Karlin, 1998; Wilson et al., 2000; Karlin, 2001; Lin and Chen, 2003). We first used two different MTS reagents, MTSES and MTSEH, to dissect out these two variables. MTSES carries a negative charge while MTSEH is neutral. The accessibility of the introduced cysteine to MTSEH should not be affected by the electrostatic attraction/repulsion from the charge or by the membrane electric field (Wilson et al., 2000). Therefore, an alteration of the MTSEH modification rate reflects the change in the thiol reactivity. On the other hand, a change in the MTSES modification rate could indicate a change in the thiol reactivity or the electrostatic attraction/repulsion force or both.

TABLE I

Permeability Ratios of Various Anions in the WT CLC-0, K149L, and K149R Mutants

		SCN^-	Cl^-	Br^-	NO_3^-	I^-	F^-
WT ($n = 3$)	E_{rev} (mV)	7.1 ± 0.4	0.1 ± 0.0	−9.8 ± 0.3	−17.2 ± 0.6	−38.9 ± 1.1	−77.0 ± 3.5
	P_X/P_{Cl}	1.33 ± 0.02	–	0.68 ± 0.01	0.51 ± 0.01	0.22 ± 0.01	0.05 ± 0.01
K149L ($n = 4$)	E_{rev} (mV)	20.6 ± 0.6	0.4 ± 0.1	−1.3 ± 0.1	−2.6 ± 0.1	−19.6 ± 2.4	−39.8 ± 2.9
	P_X/P_{CL}	2.25 ± 0.05	–	0.95 ± 0.00	0.90 ± 0.01	0.47 ± 0.04	0.21 ± 0.02
K149R ($n = 4$)	E_{rev} (mV)	11.5 ± 2.0	0.4 ± 0.2	−3.6 ± 0.7	−4.8 ± 0.6	−16.5 ± 1.9	−44.6 ± 2.6
	P_X/P_{Cl}	1.59 ± 0.12	–	0.87 ± 0.02	0.83 ± 0.02	0.53 ± 0.04	0.18 ± 0.02

Shown in Fig. 9 A are the time courses of MTSES modifications of Y512C in the WT background and in the presence of G352E, H401E, and K149L mutations. The modification time courses of these channels by MTSEH are illustrated in Fig. 9 B. The calculated modification rates from several patches are averaged and plotted in Fig. 9 C. G352E and H401E mutations introduce a negative charge to the channel, but the mutations have very little effect in altering the MTSES or the MTSEH modification rates, indicating that a negative charge at these two positions does not exert enough electrostatic potential in changing the reactivity of cysteine at Y512 position. Nor does the negative charge reduce the accessibility of MTSES modification. On the other hand, the K149L mutation reduces the MTSES modification rate of Y512C by approximately ninefold (Fig. 9 A). However, the same mutation has almost no effect on the MTSEH modification rate of Y512C (Fig. 9 B). These results are consistent with an idea that the K149L mutation may remove a positive electrostatic force in the pore region of ClC-0.

To further explore the electrostatic effect generated by K149, we compare the modification rates of Y512C when various amino acids are placed at position 149: K149 (WT), K149R, K149L, and K149A. In this series of double mutants, introduction of the Y512C mutation does not change the shift of P_o-V curves caused by the various K149 mutations (unpublished data). Three MTS reagents were applied: MTSES, MTSEH, and a positively charged reagent MTSEA. If the charge at position 149 indeed exerts an electrostatic force in the pore of CLC-0, K149L and K149A mutations should decrease the MTSES modification rates, while the same mutations should increase the MTSEA modification rates. Fig. 9 D illustrates the modification rate constants of MTSES, MTSEH, and MTSEA in these mutants. When a negatively charged modifier is used, removing the positive charge at this position reduces the modification rate. On the other hand, the same charge mutations increase the modification rate of MTSEA, a positively charged MTS reagent, while the modification rate of the neutral MTSEH is nearly unaffected.

DISCUSSION

We have examined the functional consequences of the mutations of G352, H401, and K149 in ClC-0. These three residues correspond to N318, R340, and K131 of ClC-ec1, respectively (Dutzler et al., 2002). In the ClC-ec1 structure, N318 and R340 are located at positions closer to the extracellular side, while K131 is close to S107 and Y445, two residues critical in coordinating the bound Cl^- at S_{cen} (Dutzler et al., 2002; Dutzler et al., 2003). Although all three residues do not immediately line the ion transport pathway, a through-space electrostatic effect may still be important. Theoretical calculations based on the bacterial ClC-ec1 structure suggested that the charge at these three positions might contribute to the Cl^--binding energy in the ion transport pathway. Examination of these three residues in ClC-0 reveals that K149 appears to be the most critical residue among the three. Both the gating and permeation properties are significantly affected by mutations at this position. On the other hand, mutations of G352 have no effect on the channel properties. A charge mutation at this position (G352E) does not alter the channel properties, nor does it change the modification rate of Y512C by either the charged or neutral MTS reagents.

The mutational consequence of H401E is larger than that of the G352E mutation in ClC-0. The single-channel conductance of the H401E pore is reduced to ~50% that of the WT pore. In addition, the mutation results in a rectification for the outward Cl^- flux (inward current rectification). However, this mutation produces very little gating effect, an observation that argues against the idea that the residue plays a role in coordinating the Cl^- at the S^*_{ext}, a hypothetical site thought to be important for the $[Cl^-]_o$-dependent fast-gating mechanism (Faraldo-Gomez and Roux, 2004). However, the effects of the H401E mutation on the ion-permeation properties, specifically, the reduction of the single-channel conductance and the inward rectification of the open-channel current, are similar to the predicted permeation effects exerted by an externally positioned, negatively charged residue, although it was hypothesized that such effects occurred from a charge mutation at the G352 position of ClC-0 (Corry et al., 2004). As H401E mutation introduces a fixed negative charge to the channel, the electrostatic potential from this negative charge could destabilize the Cl^- in the pore. It could also raise the energy barrier that a Cl^- ion must overcome to permeate through the pore.

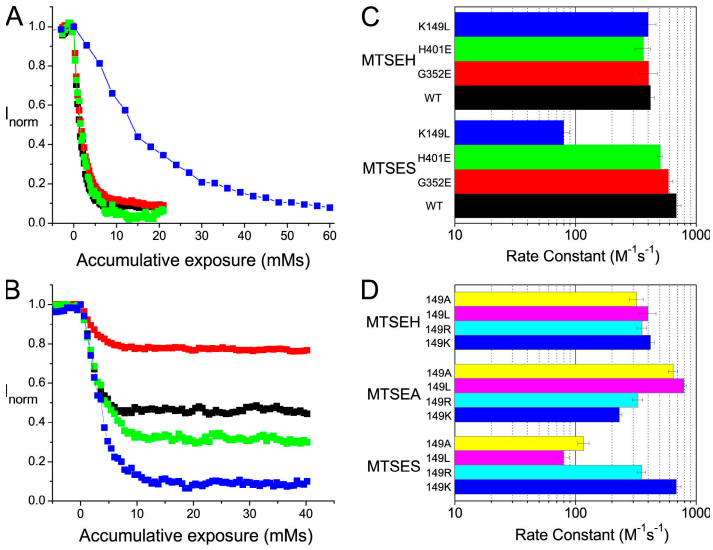

Figure 9. Effects of charge mutations of ClC-0 on the MTS modification rates of Y512C mutants. (A) MTSES modification process of Y512C in the presence of WT, G352E, H401E, or K149L background. The color codes are: black, Y512C/WT; red, Y512C/G352E; green, Y512C/H401E; blue, Y512C/K149L. (B) MTSEH modification time course of the same mutants as in A. (C) Calculated rate constants of MTSES and MTSEH modifications of the mutants shown in A and B. Note that the K149L mutation significantly alters the MTSES modification rate but not the MTSEH modification rate. Color codes of different mutants in B and C are the same as that in A. (D) Rate constants of MTSES, MTSEH, and MTSEA modifications of Y512C in the presence of various amino acids at position 149 as indicated.

In comparison with the mutations of G352E and H401E, the K149L mutation generates the largest effects on the channel functions. Faraldo-Gomez and Roux reported that the positively charged side chain of K131 of ClC-ec1 contributed a significant electrostatic force to stabilize the bound Cl^- at all Cl^--binding sites in the ion transport pathway. The residue also played a critical role in stabilizing the pore geometry by simultaneously hydrogen bonding with the carbonyl oxygen atoms of Gly106 and Ser107 (Faraldo-Gomez and Roux, 2004). A recent experiment indeed showed that the K131M mutation of ClC-ec1 resulted in a perturbation of the Cl^--H^+ antiporter function (Accardi et al., 2005), supporting the prediction for the important role of this residue in the bacterial ClC molecule. In ClC-0, after making the K149L mutation, the P_o-V curve of the mutant channel shifts to the more depolarized potential by >80 mV. In addition, the relative permeability ratios of anions are altered; all tested anions have an increased permeability ratio in the mutant. Although the exact mechanism underlying the reduced selectivity of the mutant channel for Cl^- may be complicated, one possibility could be that electrostatics plays a less important role in the mutant pore since the difference of permeability ratios between the WT channel and any of the two mutant channels in Table I is larger than the difference between K149R and K149L. The comparison between K149A and K149L is also interesting. The lysine to alanine mutation (K149A) shifts the P_o-V curve quite significantly (~60 mV), but this mutational effect is smaller than that of K149L. The unequal degrees in shifting the P_o-V curve in the K149A and K149L mutants appear to be consistent with the idea that K149 plays a structural role to maintain proper channel functions.

In addition to maintaining the pore structure, does the residue K149 also exert an electrostatic influence in the pore of ClC-0? In comparison to the effects generated by the K149L mutation, a charge-conserved mutation, K149R, creates a less robust effect both in the shift of the P_o-V curve (by ~30–40 mV) and in the change of the permeability ratios. This may suggest an electrostatic control of K149 in ClC-0 functions. Nonetheless, we employ the MTS modification approach to directly answer the question. In theory, both the reactivity and the accessibility of a pore cysteine to MTS reagents could be affected by the intrinsic electrostatic potential in the pore (Karlin, 2001). When the potential is more negative, the reactivity and the accessibility to the negatively charged MTS reagent could be reduced. Experimental evidence indeed shows that the K149L and K149A mutation results in an approximately seven- to ninefold reduction in the MTSES modification rate but increases the MTSEA modification rate by approximately three- to fourfold (Fig. 9 D). The same mutations, however, do not alter the modification rate of Y512C by a neutral MTS reagent, MTSEH. These results suggest that the reduction in the MTSES modification rate and the increase in the MTSEA modification rate may come from an effect on the accessibility of MTS reagents, while the reactivity of the free thiol of Y512C is not affected. It is interesting that the K149R exhibits a slightly slower (approximately twofold) MTSES modification rate and a slightly faster (~1.5-fold) MTSEA modification rate when compared with the WT channel. The charge on the arginine side chain is not as localized as that on the lysine side chain. Therefore, the electrostatic effect from an arginine side chain could be slightly weaker. Thus, these results support that the electrostatic force from the positively charged K149 side chain attracts the negatively charged MTS reagent to the ClC-0 pore, while it repels the positively charged MTS molecule. The same electrostatic force therefore should also alter the accessibility of Cl^- ion to the pore, an idea consistent with theoretical calculations. In contrast, the G352E and H401E mutations

do not alter the MTSES or the MTSEH modification rates. Mostly likely, the electrostatic force from the negative charge at these two positions does not extend its influence far enough to affect the MTS reagents. This is quite likely because the charge on the MTS molecules is located at the end of the MTS molecule that is probably 8–10 Å away from S_{cen} when the reactive end of the molecule attacks the thiol of Y512C. Thus the reduction of single-channel conductance found in the H401E mutant may suggest that this effect is due to an electrostatic potential change localized at the external pore mouth, if not from a nonelectrostatic, structural perturbation.

Although we have experimentally confirmed that the side chain of K149 indeed exerts an electrostatic force to the pore region of ClC-0, the exact mechanisms explaining how such an electrostatic force controls the gating and permeation functions of ClC-0 are still murky. At the single-channel level, the K149L mutation generates flickery opening events (Fig. 7 C). It is not known if this effect results from a fast channel block, a perturbation of ion binding in the pore, or simply the instability of the channel in maintaining the open pore structure. Comparing the degree of mutational consequences, it is tempting to conclude that the effects generated by the K149R mutation are due to a structural effect while the differences between those of K149L and K149R result from an electrostatic effect. We refrain ourselves to make such a simple conclusion because the charge on an arginine residue is not as localized as that of a lysine residue. Therefore, the mutational consequences seen in the K149R mutant could still partly come from an electrostatic perturbation of the WT pore.

One interesting observation in the mutants of K149 is that the mutations mostly reduce the opening rate but not the closing rate of the fast gate (Fig. 7), an effect similar to the reduction of $[Cl^-]_o$ on the fast-gating mechanism. Faraldo-Gomez and Roux (2004) suggested that K131 and R340 of the ClC-ec1 are positioned in a twofold pseudo symmetry manner, and the positive charge from these two residues together with that of R147 (corresponding to K165 of ClC-0) could stabilize the Cl^- at a binding site not identified in the crystal structure. This most externally positioned binding site (the aforementioned S^*_{ext} site) may correspond to the functional Cl^--binding site important for the external Cl^- to open the fast gate (Chen and Miller, 1996). As the opening rate of the ClC-0 is tightly controlled by $[Cl^-]_o$, the right shift of the P_o-V curve upon mutations of K149 seems to be consistent with such an idea. However, the degrees of the right shift in P_o-V curves upon reducing $[Cl^-]_o$ are approximately the same for the WT channel and the K149L mutant. In both channels, reducing $[Cl^-]_o$ by 10-fold roughly shifts the P_o-V curve by ~40 mV (unpublished data). These results may suggest that the K149L mutation does not eliminate the $[Cl^-]_o$-dependent fast-gating mechanism but only lead to a higher energy barrier for the bound Cl^- to open the fast gate. Further studies on the gating properties of the mutants of K149 should be useful for exploring the control of the fast-gate opening mechanism of ClC-0 by extracellular Cl^-.

We thank Drs. Tzyh-Chang Hwang and Jie Zheng for critical readings and comments on the manuscript.

This work was supported by a National Institutes of Health research grant (GM65447).

Olaf S. Andersen served as editor.

Submitted: 17 November 2005
Accepted: 13 March 2006

REFERENCES

Accardi, A., L. Kolmakova-Partensky, C. Williams, and C. Miller. 2004. Ionic currents mediated by a prokaryotic homologue of CLC Cl^- channels. *J. Gen. Physiol.* 123:109–119.

Accardi, A., and C. Miller. 2004. Secondary active transport mediated by a prokaryotic homologue of ClC Cl^- channels. *Nature.* 427:803–807.

Accardi, A., M. Walden, W. Nguitragool, H. Jayaram, C. Williams, and C. Miller. 2005. Separate ion pathways in a Cl^-/H^+ exchanger. *J. Gen. Physiol.* 126:563–570.

Bauer, C.K., K. Steinmeyer, J.R. Schwarz, and T.J. Jentsch. 1991. Completely functional double-barreled chloride channel expressed from a single *Torpedo* cDNA. *Proc. Natl. Acad. Sci. USA.* 88:11052–11056.

Bostick, D.L., and M.L. Berkowitz. 2004. Exterior site occupancy infers chloride-induced proton gating in a prokaryotic homolog of the ClC chloride channel. *Biophys. J.* 87:1686–1696.

Chen, M.F., and T.Y. Chen. 2001. Different fast-gate regulation by external Cl^- and H^+ of the muscle-type ClC chloride channels. *J. Gen. Physiol.* 118:23–32.

Chen, M.F., and T.Y. Chen. 2003. Side-chain charge effects and conductance determinants in the pore of ClC-0 chloride channels. *J. Gen. Physiol.* 122:133–145.

Chen, T.Y. 1998. Extracellular zinc ion inhibits ClC-0 chloride channels by facilitating slow gating. *J. Gen. Physiol.* 112:715–726.

Chen, T.Y. 2005. Structure and function of clc channels. *Annu. Rev. Physiol.* 67:809–839.

Chen, T.Y., M.F. Chen, and C.W. Lin. 2003. Electrostatic control and chloride regulation of the fast gating of ClC-0 chloride channels. *J. Gen. Physiol.* 122:641–651.

Chen, T.Y., and C. Miller. 1996. Nonequilibrium gating and voltage dependence of the ClC-0 Cl^- channel. *J. Gen. Physiol.* 108:237–250.

Cohen, J., and K. Schulten. 2004. Mechanism of anionic conduction across ClC. *Biophys. J.* 86:836–845.

Corry, B., M. O'Mara, and S.H. Chung. 2004. Conduction mechanisms of chloride ions in ClC-type channels. *Biophys. J.* 86:846–860.

Dutzler, R., E.B. Campbell, M. Cadene, B.T. Chait, and R. MacKinnon. 2002. X-ray structure of a ClC chloride channel at 3.0 Å reveals the molecular basis of anion selectivity. *Nature.* 415:287–294.

Dutzler, R., E.B. Campbell, and R. MacKinnon. 2003. Gating the selectivity filter in ClC chloride channels. *Science.* 300:108–112.

Engh, A.M., and M. Maduke. 2005. Cysteine accessibility in ClC-0 supports conservation of the ClC intracellular vestibule. *J. Gen. Physiol.* 125:601–617.

Estevez, R., B.C. Schroeder, A. Accardi, T.J. Jentsch, and M. Pusch. 2003. Conservation of chloride channel structure revealed by an inhibitor binding site in ClC-1. *Neuron.* 38:47–59.

Faraldo-Gomez, J.D., and B. Roux. 2004. Electrostatics of ion stabilization in a ClC chloride channel homologue from *Escherichia coli*. *J. Mol. Biol.* 339:981–1000.

Hanke, W., and C. Miller. 1983. Single chloride channels from *Torpedo electroplax*. Activation by protons. *J. Gen. Physiol.* 82:25–45.

Jentsch, T.J., M. Poet, J.C. Fuhrmann, and A.A. Zdebik. 2005. Physiological functions of CLC Cl^- channels gleaned from human genetic disease and mouse models. *Annu. Rev. Physiol.* 67:779–807.

Karlin, A. 2001. Scam feels the pinch. *J. Gen. Physiol.* 117:235–238.

Lin, C.W., and T.Y. Chen. 2000. Cysteine modification of a putative pore residue in ClC-0: implication for the pore stoichiometry of ClC chloride channels. *J. Gen. Physiol.* 116:535–546.

Lin, C.W., and T.Y. Chen. 2003. Probing the pore of ClC-0 by substituted cysteine accessibility method using methane thiosulfonate reagents. *J. Gen. Physiol.* 122:147–159.

Lin, Y.W., C.W. Lin, and T.Y. Chen. 1999. Elimination of the slow gating of ClC-0 chloride channel by a point mutation. *J. Gen. Physiol.* 114:1–12.

Ludewig, U., M. Pusch, and T.J. Jentsch. 1996. Two physically distinct pores in the dimeric ClC-0 chloride channel. *Nature.* 383:340–343.

Maduke, M., C. Miller, and J.A. Mindell. 2000. A decade of CLC chloride channels: structure, mechanism, and many unsettled questions. *Annu. Rev. Biophys. Biomol. Struct.* 29:411–438.

Middleton, R.E., D.J. Pheasant, and C. Miller. 1996. Homodimeric architecture of a ClC-type chloride ion channel. *Nature.* 383:337–340.

Miller, C. 1982. Open-state substructure of single chloride channels from *Torpedo electroplax*. *Philos. Trans. R. Soc. Lond. B Biol. Sci.* 299:401–411.

Miller, C., and M.M. White. 1984. Dimeric structure of single chloride channels from *Torpedo electroplax*. *Proc. Natl. Acad. Sci. USA.* 81:2772–2775.

Miloshevsky, G.V., and P.C. Jordan. 2004. Anion pathway and potential energy profiles along curvilinear bacterial ClC Cl^- pores: electrostatic effects of charged residues. *Biophys. J.* 86:825–835.

Pascual, J.M., and A. Karlin. 1998. State-dependent accessibility and electrostatic potential in the channel of the acetylcholine receptor. Inferences from rates of reaction of thiosulfonates with substituted cysteines in the M2 segment of the α subunit. *J. Gen. Physiol.* 111:717–739.

Picollo, A., and M. Pusch. 2005. Chloride/proton antiporter activity of mammalian CLC proteins ClC-4 and ClC-5. *Nature.* 436:420–423.

Pusch, M., and T.J. Jentsch. 2005. Unique structure and function of chloride transporting CLC proteins. *IEEE Trans Nanobioscience.* 4:49–57.

Saviane, C., F. Conti, and M. Pusch. 1999. The muscle chloride channel ClC-1 has a double-barreled appearance that is differentially affected in dominant and recessive myotonia. *J. Gen. Physiol.* 113:457–468.

Scheel, O., A.A. Zdebik, S. Lourdel, and T.J. Jentsch. 2005. Voltage-dependent electrogenic chloride/proton exchange by endosomal CLC proteins. *Nature.* 436:424–427.

Wilson, G.G., J.M. Pascual, N. Brooijmans, D. Murray, and A. Karlin. 2000. The intrinsic electrostatic potential and the intermediate ring of charge in the acetylcholine receptor channel. *J. Gen. Physiol.* 115:93–106.